Cross sections and collision dynamics of the excitation of $(1snp)\ ^1P^o$ levels of helium, $n=2-5$, by intermediate- and high-velocity electron, proton, and molecular-ion (H_2^+ and H_3^+) impact

H. Merabet,[1] M. Bailey,[1] R. Bruch,[1] J. Hanni,[1] S. Bliman,[2] D. V. Fursa,[3] I. Bray,[3] K. Bartschat,[4] H. C. Tseng,[5] and C. D. Lin[6]
[1]*Department of Physics, University of Nevada Reno, Reno, Nevada 89557*
[2]*Department de Physique, University de Marne la Vallée, 96166 Noisy LeGrand, France*
[3]*Centre for Atomic, Molecular and Surface Physics, School of Mathematical and Physical Sciences, Murdoch University, Perth 6150, Australia*
[4]*Department of Physics and Astronomy, Drake University, Des Moines, Iowa 50311*
[5]*Department of Physics, Chung Yuan Christian University, Chung Li, 32023 Taiwan*
[6]*Department of Physics, Kansas State University, Manhattan, Kansas 66506-2601*
(Received 26 April 2000; revised manuscript received 7 September 2000; published 8 June 2001)

Experimental cross sections in the extreme ultraviolet (EUV) wavelength range for the excitation of helium following electron and H^+, H_2^+, and H_3^+ ion impact are presented for He I $(1snp)\ ^1P^o$ states with $n=2-5$. These measurements extend over large velocity ranges 3.8–8.5 a.u. for electrons, 1.4–7.5 a.u. for protons, and 1.4–4.0 a.u. for H_2^+ and H_3^+ ions, respectively, and represent the most complete data set obtained so far in the EUV. Furthermore, the methods of convergent close coupling and *R* matrix with pseudostates have been used here to predict excitation cross sections for the He I $(1snp)\ ^1P^o$ states following electron impact and the atomic-orbital close-coupling expansion for proton impact. In particular, our theoretical results are presented and compared with our EUV experimental cross sections for equal projectile velocities together with previous experimental results, including cross sections derived from scaling procedures. The electron cross sections are found to deviate from the proton data at intermediate and lower energies ($v<3.8$ a.u.).

DOI: 10.1103/PhysRevA.64.012712 PACS number(s): 34.80.Bm, 34.80.Dp, 34.50.Fa

I. INTRODUCTION

Cross-section measurements of processes involving helium by electron and ion impact are fundamental to the investigation of few-electron interactions in atomic and ionic collision physics [1–3]. Knowledge of such collision processes is important not only for the understanding of the collision dynamics but also for laboratory and astrophysical plasmas and helium-based radiation diagnostics such as solar flare analysis [4–12]. Similar collision processes depend on a large parameter space which includes projectile velocity, size, charge states, charge sign, mass, and structural complexity.

The processes investigated in this study are

$$e^- + \mathrm{He} \rightarrow \mathrm{He}(1snp)\ ^1P^o + e^- \qquad (1)$$
$$\searrow$$
$$\mathrm{He}(1s^2)\ ^1S^o + h\nu,$$

and

$$H_m^+ + \mathrm{He} \rightarrow \mathrm{He}(1snp)\ ^1P^o + H_m^+ \ \text{(or fragments)} \quad (m=1-3) \qquad (2)$$
$$\searrow$$
$$\mathrm{He}(1s^2)\ ^1S^o + h\nu$$

(fragments are H_2^+, H^+, H, H^-, and projectile e^-), where the emitted extreme ultraviolet (EUV) radiation is observed at 90° with respect to the projectile beam.

Theoretically, the excitation of helium by charged-particle impact at high velocities ($v>3.8$ a.u.) has been well described in terms of the first Born approximation and the Bethe theory [13,14]. In the intermediate-energy range, where the cross sections exhibit their maximum values, all previous theoretical calculations [15–17] are not in agreement with the measured cross sections for electron and proton impact. Therefore, we have applied here three theoretical techniques, namely, the methods of convergent close coupling (CCC) [18,19], *R* matrix with pseudostates (RMPS) [20,21], and atomic-orbital close coupling (AOCC) [22], in an attempt to elucidate the excitation mechanisms of helium following electron and proton impact for a wide range of projectile velocities (1–9 a.u.). In this connection, we note that the convergent close-coupling method used earlier by Fursa and Bray [18] for lower excited levels $(1snp)\ ^1P^o$ ($n=2$ and 3) for the electron impact has been successfully extended in this work to include transitions to higher Rydberg states with $n>3$. A similar method (AOCC) has also been utilized to derive excitation cross sections for He I $(1snp)\ ^1P^o$ states for the H^++He collision system [22]. In addition we introduce theoretical data for the He I $(1s2p)\ ^1P^o$ levels following electron impact obtained using the *R* matrix with pseudostates method for incident energies ranging from 30 up to 400 eV (i.e., $1.4 \leqslant v \leqslant 5.4$ a.u.). The theoretical results pre-

sented in this paper show excellent agreement with most of our EUV and other experimental data.

To our knowledge, the cross-section measurements presented in this paper are the most comprehensive results obtained for electron and H_n^+ ion projectiles ($n=1-3$) under identical experimental conditions in the EUV wavelength range. A comparison of our cross-section data for electron and proton projectiles with earlier data obtained in the visible and UV spectral regions extends over the velocity range from 1 to 9 a.u. Furthermore, molecular projectiles (H_2^+ and H_3^+) have been utilized in an effort to compile additional information concerning the excitation process for helium associated with projectile charge state, mass, geometry, and velocity. For H_n^+ ions, where theoretical descriptions are nonexistent, a comparison is made with a simple scaling model [23]. Moreover, cross-section ratios for H_n^+ impact, $\sigma^*(H_n^+)$ ($n=1-3$), and scaled proton results, $n\sigma^*(H^+)$, are compared in order to observe molecular contributions to the excitation of the He target by the additional projectile electrons carried into the collision process.

In the following, we describe the experimental method utilized for the EUV measurements (Sec. II). Then, in Sec. III, we give a brief description of the three theoretical procedures, i.e., CCC, RMPS, and AOCC, used in this work for the calculations of excitation cross sections. We have listed all our experimental (corrected for polarization effects) and theoretical results in Sec. IV. Specifically, we provide a detailed discussion and comparison of all data for e^-+He and H^++He collision systems. In this section we also focus on the molecular-ion (H_2^+ and H_3^+) impact results and compare them with the corresponding proton data.

II. EXPERIMENTAL SETUP

A. Description of the apparatus and cross-section determination

The experimental setup has been described in detail by Bailey *et al.* [24,25], and therefore only a brief discussion is presented here. Positive-ion beams (H^+, H_2^+, and H_3^+) produced by the University of Nevada Reno 2 MV Van de Graaff accelerator and electron beams created by an electron gun deliver projectile beams focused into a differentially pumped target cell. The EUV emission was observed at right angles to the projectile beam and analyzed with a 1.5-m grazing-incidence monochromator in conjunction with a channeltron detector. For 100-μm slit widths, the monochromator provided a spectral linewidth (full width at half maximum) of 0.1 nm at $\lambda=30.4$ nm; corresponding to a spectral resolution of $(\lambda/\Delta\lambda)\approx 304$.

Cross sections for the excitation of He measured in this work were put on an absolute scale by normalizing our measured high-velocity cross-section data to the Bethe-Born cross-section values for electron and proton impact velocities $v>3.8$ a.u. Indeed, the accuracy of cross sections for the excitation of helium is typically judged in terms of their agreement with the Bethe theory at high impact energies; it seems reasonable that the Bethe cross-section results may be directly used as reference values. This allowed us to determine the detection sensitivity for the wavelength region from 51 to 59 nm [He I $(1snp)\ ^1P^o \rightarrow (1s^2)\ ^1S$] and to effectively cross-calibrate this region with the corresponding 22–31 nm range [He II $(np)\ ^2P^o \rightarrow (1s)\ ^2S$]. The comparison has been restricted to projectile energies $E\geqslant 200$ eV for electrons and $E\geqslant 368$ keV for protons ($v\geqslant 3.8$ a.u.) since the Bethe formula is not considered to be very accurate below these energies (Donaldson, Hender, and McConkey [26]). A complete description of the procedure is given by Bailey *et al.* [24]. The excellent agreement of our cross sections with the benchmark results of Hippler and Schartner [27], Westerveld, Heideman, and van Eck [28], and Donaldson *et al.* [26] supports the hypothesis that this method is valid.

B. Different sources of errors

Our previous measurements of EUV cross sections associated with the subsequent decay to the $(1s^2)\ ^1S$ ground state via electric dipole transitions may be affected by different sources of error. Such errors are due to nonlinear pressure dependence, cascade repopulation of the He I $(1snp)\ ^1P^o$ states, nonstatistical population of magnetic substates, statistics of the measurement procedure, energy uncertainty of the Van de Graaff accelerator, target pressure stability and charge normalization, etc. Some of these effects are discussed in detail below.

1. Pressure and cascade population effects

Nonlinear pressure dependencies resulting from resonant absorption are experienced at the target pressures used in this study. Hence additional detailed measurements of line intensity as a function of target pressure over the range from 0.1 to 150 mtorr were performed for all $n\ ^1P^o$ states decaying to the He I $(1s^2)\ ^1S$ ground state. The uncertainties associated with these obtained corrections are approximately 5%. Moreover, corrections to the measured line intensity were made to account for cascade repopulation. Additional corrections to the integrated charge were considered when using molecular H_2^+ and H_3^+ ions and electrons as projectiles where fragmentation and scattering of the projectile can effect charge normalization.

The proton results for projectile velocities from 1.4 to 2.5 a.u. (energies from 50 to 150 keV) have been corrected for cascade effects using the values of van den Bos and coworkers [15] for He I $(1snp)\ ^1P^o$ levels, $n=3-5$. Corrections for the He I $(1s2p)\ ^1P^o$ level were calculated by Stolte and Bruch [29,30] from the same data. These cascade corrections vary from 7.5% to 22%, 6% to 16%, 6% to 18%, and 4% to 12% for the $(1s2p)\ ^1P^o$, $(1s3p)\ ^1P^o$, $(1s4p)\ ^1P^o$, and $(1s5p)\ ^1P^o$ levels, respectively. For the He I $(1s4p)\ ^1P^o$ results at 150 keV, the cascade correction is 6% from van den Bos *et al.* [15] and 3.9% from Hippler and Schartner [27]; therefore an average of these values was used in this case. The He I $(1s5p)\ ^1P^o$ corrections for energies greater than 150 keV were estimated from the results of Hippler and Schartner [27] and range from 2% to 4%.

2. Polarization effects

The preferential beamlike properties of our excitation mechanism lead to polarized emission of the observed He I

$(1snp)\ ^1P^o \rightarrow (1s^2)\ ^1S^o$ transitions. This process is energy dependent [31] and is particularly important at threshold and low impact energies for electron impact where the polarization may change rapidly with energy [31,32].

The corresponding uncertainties due to polarization give rise to a nonisotropic population of the He I $(1snp)\ ^1P^o$-magnetic substates ($M_L = 0, \pm 1$). The angular distribution of the observed intensity in the 52–59 nm wavelength range is given by [33]

$$I(\theta) = I_0\{1 + A_2 P_2(\cos\theta)\}, \tag{3}$$

where A_2 is the alignment parameter of the $^1P^o$ state, $P_2(\cos\theta)$ is the second Legendre polynomial, θ is the observation angle, I_0 is the intensity for isotropic distribution, and $I(\theta)$ the measured intensity. The alignment parameter A_2 is connected to the degree of linear polarization P following excitation of helium to $(1snp)\ ^1P^o$ states via [31]

$$A_2 = \frac{2P}{P-3}. \tag{4}$$

Recently, we have measured this degree of linear polarization P following excitation for $e^- + \mathrm{He}$ and $\mathrm{H}^+ + \mathrm{He}$ collisions [31,34]. Such measurements have shown that experimental values of P following excitation of helium by proton impact are much smaller than the ones for electron impact [32,34] at low impact velocities, whereas they exhibit a more pronounced decrease at intermediate- and higher-energy ranges. The correction factors owing to polarization are found to be less than 6% for electron impact [31] and less than 7% for proton impact [34].

3. Total experimental uncertainties

Statistics of the measured line intensities can introduce additional uncertainties ranging from approximately 1% for He I $(1s2p)\ ^1P^o$ up to 8% for He I $(1s5p)\ ^1P^o$ decays. When instrumental uncertainties related to energy resolution of the Van de Graaff accelerator, target pressure stability, polarization, and charge normalization are combined, total experimental uncertainties ranging from 8% for He I $(1s2p)\ ^1P^o$ to 18% for He I $(1s5p)\ ^1P^o$ are obtained.

III. THEORETICAL METHODS USED FOR EXCITATION CROSS-SECTION CALCULATIONS

Over the past 20 years, several theoretical approaches have been developed in an attempt to understand the collision dynamics of impact excitation of helium [35–37,16,17]. However, none of these techniques has succeeded in correctly reproducing the excitation cross sections of He by electron or proton impact at all energies. Until recently this problem was persistent, and reliable excitation cross sections could be calculated only in the ''low-energy regime'' below the ionization threshold or in the ''high-energy regime'' of incident energies several times above the ionization threshold for electron impact. In the former region, nonperturbative close-coupling-type expansions, most notably the well-known 5-state, 11-state, 19-state, and 29-state calculations of Berrington and co-workers [35–37], were applied, while perturbative approaches based on the Born series expansion were used in the latter [16,17]. For the ''intermediate-energy regime,'' i.e., projectile energies ranging from about one to five times the ionization threshold, however, theoretical predictions were judged to be significantly less reliable, due to coupling to high-lying discrete as well as continuum target states.

Recently, however, Fursa and Bray [18] reported a comprehensive study of e-He scattering in the incident energy range from 1.5 to 500 eV. These authors extended their CCC method to treat the helium target [19] and obtained very impressive agreement with most of the experimental data. Another success worthy of notice for the He problem at low- and intermediate-energy impact, is the R matrix with pseudostates method [20,21,38–40], which incorporates the essential idea of the CCC approach and can be applied to complex targets. In the area of atom–heavy-ion collisions, close-coupling methods in the semiclassical impact approximation have been used, expanding the time-dependent wave functions in basis functions consisting of atomic or molecular orbitals [22]. Such methods have been successfully utilized to study excitation, charge transfer, and ionization cross sections for simple collision systems.

In the present study both CCC and RMPS methods are used to predict excitation cross sections for electron impact while the atomic-orbital close-coupling expansion method is employed to treat proton impact on He. In this section, a short description of these methods is given. Further details about these calculations are given elsewhere [18–22]. The theoretical results obtained are also discussed and compared with previous calculations for both $e^- + \mathrm{He}$ and $\mathrm{H}^+ + \mathrm{He}$ collision systems at equivalent projectile velocity ranges.

A. Convergent close-coupling calculations for $e^- + \mathrm{He}$ collisions

The details of the CCC method for e-He scattering may be found in Ref. [18]. Briefly, the total wave function is expanded using a set of two-electron states obtained by diagonalizing the target Hamiltonian in an explicitly antisymmetric basis of Laguerre functions. Predominantly the frozen-core approximation is employed, where for all states one of the orbitals is the $1s$ of He^+ with the other orbital being a linear combination of Laguerre functions. The strength of this approximation is that the excited states are described quite accurately and convergence studies with increasing Laguerre basis sizes may be systematically performed. The disadvantage is that the ground state is not very accurate. Relaxing the frozen-core approximation leads to the generation of too many states to solve the subsequent coupled equations on our presently available computers. However, we may do so if we approximate the solution of the coupled equations by the (unitary or otherwise) Born or distorted-wave Born approximation. Thus, we are readily able to test the frozen-core approximation at the higher energies where the above approximations yield sufficiently accurate results.

The present results are from 89-state calculations, which were designed specifically for the current investigation and have up to $n = 6$ physical states with orbital angular momen-

tum $l<6$, in addition to negative- and positive-energy pseudostates which take into account the remaining discrete spectrum and the target continuum. These calculations yield much the same results as those published earlier for $n\leqslant 3$ states, but are more accurate for $n=4$ and 5 states. The frozen-core model was used and checked at the higher energies by comparison with the Born approximation with and without the frozen-core approximation. It was found that, once the Born approximation using the frozen-core model target structure agrees with the CCC results, the Born approximation with substantially improved target states reduces these by approximately 10%.

B. *R*-matrix calculations for e^-+He collisions

The RMPS calculation performed for the present study is an extension of the work described by Bartschat *et al.* [38] and by Hudson *et al.* [21] to higher energies. This extension was achieved by increasing the number of continuum orbitals, which are used to expand the wave function of the continuum electron inside the *R*-matrix box of 27, from 30 to 50. It thus allowed for the calculation of converged results for the $(1s^2)\,^1S^o \rightarrow (1s2p)\,^1P^o$ transition up to incident energies of 400 eV. As in the CCC model described above, the physical states (we only used the five lowest states of helium) were supplemented by a number of pseudostates (36 in this case) to represent the channel coupling to the higher-lying discrete states as well as the continuum states of the target. Note that the RMPS model yielded an excellent description of the target (relative to most other collision calculations) for both the relevant energy levels and the oscillator strengths (see Ref. [38] for details). Hence, the RMPS results are expected to be reliable over the entire energy region for which they were calculated, with the exception of resonances in the narrow window of incident energies between the physical states with $n>2$ and the ionization threshold. In particular, we note that the RMPS results would be expected to converge toward first-Born predictions obtained with an equally sophisticated target description, as soon as channel-coupling effects have dimished sufficiently to warrant such a perturbative treatment.

C. Atomic-orbital close-coupling calculations for H^++He collisions

For H^++He collisions the excitation cross sections are calculated using the standard close-coupling expansion method. By treating the Schrödinger equation for the two electrons in the Coulomb fields of the two moving nuclei, one expands the time-dependent wave function in terms of the eigenstates of He. In the energy region under study charge-transfer processes are not important so that the basis functions included are all centered around the target atom. In other words, only the helium eigenstates are used in the expansion. Following the standard procedure the resulting expansion coefficients satisfy a system of linear first-order differential equations for each collision impact parameter. The total excitation cross section to each magnetic substate is calculated by integrating the excitation probability $P(b)$ over the impact-parameter plane. Details of such calculations can be found in the review by Fritsch and Lin [22]. In this calculation basis states consist of singly excited states up to $n=3$ and some pseudostates for each total angular momentum L.

TABLE I. Experimental and theoretical cross sections for the excitation of helium by electrons for He I $(1s2p)\ ^1P^o$ states as a function of the impact velocities. The experimental EUV cross sections have been corrected for cascade effects and nonstatistical population of magnetic substates. Units are 10^{-19} cm^2.

Projectile energy (eV)	Projectile velocity (a.u.)	Experiment		Theory	
		EUV[a]	RCS[b]	CCC[c]	RMPS[d]
200	3.8	92.0±6.9	83.1±7.5	89.7	85.44
276	4.5	74.7±5.6	72.5±6.5	80.2	72.85
340	5.0	63.1±4.7	64.8±5.8	72.2	64.54
412	5.5	57.6±4.3	59.4±5.3	64.8	
500	6.1	51.9±3.9	56.7±5.1	55.4	
575	6.5	45.9±3.4	51.8±4.7	52.8	
667	7.0	46.2±3.5	45.6±4.1	47.2	
735	7.3	39.6±3.0	42.2±3.8	44.4	
836	7.8	34.4±2.6	37.2±3.3	39.8	

[a]Extreme ultraviolet measurements, this work.
[b]Recommended cross sections from de Heer [11].
[c]Convergent close-coupling calculations, this work.
[d]*R* matrix with pseudostates calculations, this work.

IV. RESULTS AND DISCUSSION

Our EUV cross-section results for electron and proton impact are summarized and listed in Tables I–IV, where the estimated errors are also given. Precisely, in Table I (Table II) and Table III (Table IV) we exhibit our EUV results for He I $(1s2p)\ ^1P$ [He I $(1s3p)\ ^1P^o$] and compare them with previous experimental and scaled data [6–11] for electron

TABLE II. Experimental and theoretical cross sections for the excitation of helium by electrons for He I $(1s3p)\ ^1P^o$ states as a function of the impact velocities. The experimental EUV cross sections have been corrected for cascade effects and nonstatistical population of magnetic substates. Units are 10^{-19} cm^2.

Projectile energy(eV)	Projectile velocity (a.u.)	Experiment		Theory
		EUV[a]	RCS[b]	CCC[c]
200	3.8	23.9±1.8	20.8±1.9	22.1
276	4.5	18.5±1.4	18.2±1.6	19.6
340	5.0	15.5±1.2	16.4±1.5	17.8
412	5.5	14.9±1.1	14.9±1.3	16.1
500	6.1	13.9±1.0	12.9±1.2	13.7
575	6.5	11.5±0.9	11.8±1.1	12.9
667	7.0	11.7±0.9	10.4±0.9	11.7
735	7.3	11.0±0.8	10.0±0.9	11.0
836	7.8	8.4±0.6	9.1±0.8	9.8

[a]Extreme ultraviolet measurements, this work.
[b]Recommended cross sections from de Heer [11].
[c]Convergent close-coupling calculations, this work.

TABLE III. Comparison of experimental and theoretical cross sections for the excitation of helium by protons for He I $(1s2p)$ $^1P^o$ states as a function of the projectile velocity. Our experimental EUV cross sections have been corrected for cascade effects. Units are 10^{-19} cm^2.

Projectile energy (eV)	Projectile velocity (a.u.)	Experiment		Theory
		EUV[a]	RCS[b]	AOCC[c]
50	1.4	85.8±7.7	79.3±15.8[d]	92.84
100	2.0	181.0±16.3	127.3±25.4[d]	155.85
156	2.5	122.5±11.0	128.1±19.2[e]	143.57
200	2.8		121.1±10.9[e]	130.08
225	3.0	112.8±10.2	115.5±10.4[e]	123.14
307	3.5	92.7±8.3	101±9.1[e]	106.97
368	3.8	87.7±7.9	91.6±8.2[e]	97.31
400	4.0	80.4±7.2	86.4±7.8[e]	93.31
500	4.5		78.8±7.1[e]	82.50
626	5.0	67.6±6.1	67.6±6.1[e]	70.21
700	5.3		64.7±5.8[e]	65.20
800	5.7		56.8±5.1[e]	60.39
916	6.0	45.6±4.1	53.5±4.8[e]	56.67
1000	6.3		50.5±4.5[e]	50.13
1400	7.5	38.0±3.4		36.55

[a]Extreme ultraviolet measurements, this work.
[b]Recommended cross sections from de Heer *et al.* [7].
[c]Atomic orbital close-coupling calculations, this work.
[d]Values taken from the optical experiment of van den Bos *et al.* [15].
[e]Values taken from the optical experiment of Hippler and Schartner [27].

TABLE IV. Comparison of experimental and theoretical cross sections for the excitation of helium by protons for He I $(1s3p)$ $^1P^o$ states as a function of the projectile velocity. Our experimental EUV cross sections have been corrected for cascade effects. Units are 10^{-19} cm^2.

Projectile energy(eV)	Projectile velocity (a.u.)	Experiment		Theory
		EUV[a]	RCS[b]	AOCC[c]
50	1.4	18.5±1.7	19.4±3.8[d]	23.44
100	2.0	40.3±3.6	31.1±6.2[d]	43.02
156	2.5	29.8±2.7	31.9±4.8[e]	38.42
200	2.8		29.9±2.7[e]	33.49
225	3.0	27.0±2.4	28.7±2.6[e]	30.75
307	3.5	23.1±2.1	25.3±2.3[e]	26.59
368	3.8	24.1±2.2	23.3±2.1[e]	24.07
400	4.0	21.0±1.9	22.0±2.0[e]	24.34
500	4.5		19.7±1.8[e]	20.91
626	5.0	15.7±1.4	17.5±1.6[e]	17.29
700	5.3		16.5±1.5[e]	16.24
800	5.7		15.0±1.4[e]	14.74
916	6.0	12.3±1.1	13.9±1.3[e]	13.21
1000	6.3		12.9±1.2[e]	12.63
1400	7.5	10.4±0.9		9.55

[a]Extreme ultraviolet measurements, this work.
[b]Recommended cross sections from de Heer *et al.* [7].
[c]Atomic orbital close-coupling calculations, this work.
[d]Values taken from the optical experiment of van den Bos *et al.* [15].
[e]Values taken from the optical experiment of Hippler and Schartner [27].

and proton impact, respectively. We have also plotted the corresponding cross sections for the He I $(1snp)$ $^1P^o$ levels, $n=2-5$, in Figs. 1 and 2 for electron and proton impact, respectively. An overview of the cross sections for He I $(1snp)$ $^1P^o$ states for electron and proton impact is presented in Fig. 3 as a function of projectile velocity in atomic units, where we have included previously obtained results by other workers [15,26–28,41,42].

To date, several experiments and theories (see Sec. III) have been devoted to the study of excitation processes of helium by positively and negatively charged projectiles. Hence, it is of great interest to make a comprehensive comparison of our EUV experimental and theoretical results with previous data for e^-+He and H^++He collisions. This aspect is the main focus in the following sections.

A. e^-+He and H^++He collisions

In the intermediate-velocity range, excitation of He by proton and electron impact is a complex many-body problem requiring sophisticated theoretical approaches beyond the first Born approximation. To elucidate the collision dynamics in the intermediate-velocity range we analyze the excitation cross-section dependence on different projectile velocities. First we consider the e^-+He case.

The EUV experimental and CCC and RMPS theoretical excitation cross sections for electron impact on helium are shown in Tables I and II and plotted in Fig. 1. The 89-state CCC calculations shown in this figure have been done specifically for He I $(1snp)$ $^1P^o$ states with $n=2-4$ while the corresponding He I $(1s5p)$ $^1P^o$ cross sections are estimated using the $1/n^3$ scaling law. Figure 1 includes the optical experimental data of Westerveld *et al.* [28] and of Donaldson *et al.* [26], as well as the recommended experimental data by de Heer and co-workers [7,11]. Also given are our results for the improved Born approximation calculated using the same computer code as for the CCC predictions, but with a much improved target structure. As can be seen from this figure, the CCC results agree well with the EUV cross sections measured in this work, as well as with the other recommended experimental data, over the entire range of incident energies plotted. Despite this favorable assessment, however, we notice that overall the CCC method systematically overestimates the cross sections by about 10%. As pointed out in Sec. III A, this is due to the frozen-core target description used in the CCC model, which is somewhat problematic for the ground state. As expected, our improved Born approximation does not agree properly with experiment in the low- and intermediate-energy regime, but is in excellent agreement with our measurements for velocities of approximately 5 a.u. (340 eV) and above. This finding, together with the good agreement between the RMPS results (see Table I and Fig. 1) for He I $(1s2p)$ $^1P^o$ and experiment at all energies

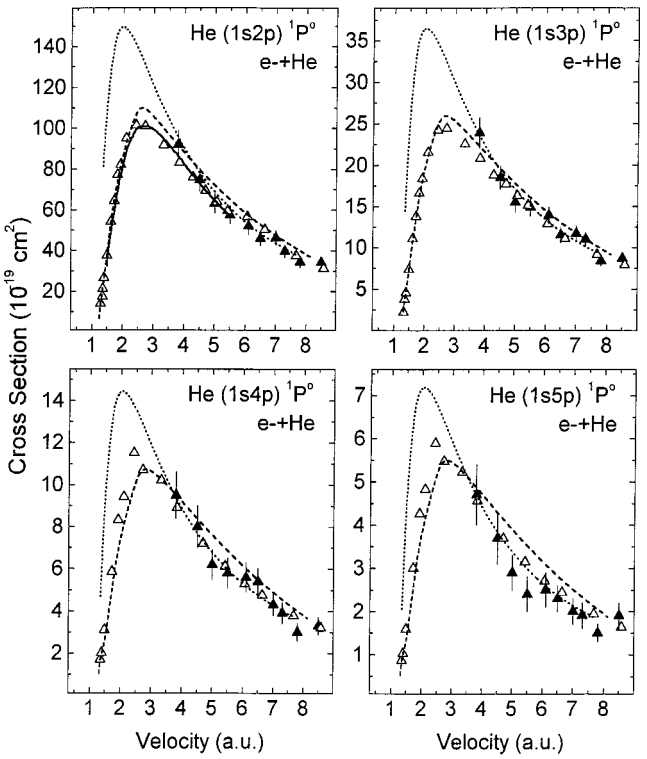

FIG. 1. Experimental cross sections (corrected for polarization effects) for He I $(1snp)$ $^1P^o$ states due to electron impact compared to recent theoretical results. Experiment: ▲, this work; △, de Heer, Hoekstra, and Summers [9]. Theory: — — —, convergent close-coupling calculation, this work; ——, R matrix with pseudostates calculations, this work; · · · ·, improved first Born approximation, this work.

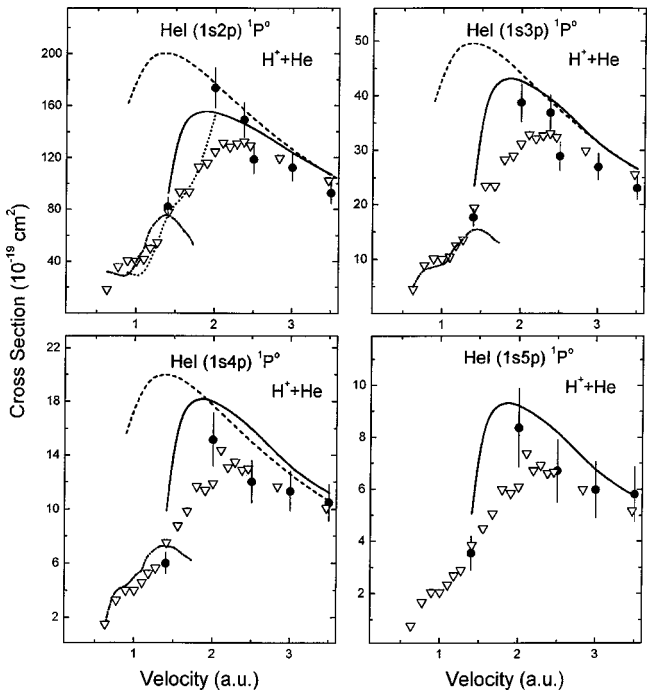

FIG. 2. Theoretical cross sections for the excitation of $(1snp)$ $^1P^o$ states in He following proton impact compared with experimental (corrected for polarization effects) and scaled results. Experiment: ●, EUV, this work; ▽, de Heer *et al.* [7]. Theory: — — —, first Born [13]; ——, atomic-orbitals close-coupling calculation, this work; · · · ·, two-electron close-coupling calculation [16]; — · — · — · —, one-electron close-coupling calculation [17].

and the apparent convergence of RMPS and improved first Born theory in the 3.8–5.5 a.u. velocity range, demonstrates that a sophisticated target description is more important than channel coupling in the high-energy regime.

Now let us consider the H^++He collisions. In Fig. 2 we exhibit our experimental data, the scaled data recommended by de Heer and co-workers [7], and the most prominent theoretical results for He I $(1snp)$ $^1P^o \rightarrow (1s^2)$ ^1S $(n=2-5)$ [9–11,16,17] for proton impact versus projectile velocity. The scaled data for proton impact consist of the earlier visible measurements of van den Bos *et al.* [15], renormalized to agree with the UV measurements of Hippler and Schartner [27] for He I $(1s3p)$ $^1P^o$ and He I $(1s4p)$ $^1P^o$. Such renormalization procedures have been performed in an attempt to compile reference cross-section data in the low- to intermediate-velocity range for fusion plasma diagnostics [7–11,17]. In the case of He I $(1s2p)$ $^1P^o$, where no optical measurements are possible, the scaled results were obtained by scaling of He I $(1s3p)$ $^1P^o$ optical data [15] by the high-velocity asymptotic ratio of the He I $(1s2p)$ $^1P^o$ and $(1s3p)$ $^1P^o$ cross sections as predicted by the Bethe-Born approximation [42].

In Fig. 2, we note that the general trend for all measured cross sections shows a moderately steep increase in cross section for small impact velocities, reaching a maximum around 2 a.u., followed by a gradual decrease with increasing projectile velocity toward the asymptotic high-energy limit. In the velocity region above 3 a.u., our EUV measurements show excellent agreement with those of Hippler and Schartner [7,27] (see Tables III and IV), confirming the validity of our normalization procedure. We have also indicated in Fig. 2 the predictions of our AOCC approach, together with other theoretical results. It is evident that all these calculations coincide with our experimental data in the higher-velocity range ($v > 2.5$ a.u.), where the AOCC cross sections go nicely toward first Born results at higher energies. However we have observed slight deviations from the experimental EUV findings. Nonetheless, the agreement of the AOCC, calculations with our EUV cross sections is reasonably good within the error bars. The AOCC calculations were performed for the He I $(1s2p)$ $^1P^o$ and He I $(1s3p)$ $^1P^o$ states explicitly; the data for the He I $(1s4p)$ $^1P^o$ and He I $(1s5p)$ $^1P^o$ states from the AOCC calculations are estimated using the $1/n^3$ rule from the former states.

In this figure, results from earlier calculations and experiments have been shown as well. The two-electron close-coupling calculations by Slim *et al.* [16] show good agreement with the scaled results of de Heer [11] for excitation to the He I $(1s2p)$ $^1P^o$ level. In contrast, the one-electron close-coupling calculations of Fritsch [17] deviate significantly above $v = 1.4$ a.u. from the scaled data, while they show marginal agreement with the renormalized visible results of van den Bos *et al.* for the He I $(1s3p)$ $^1P^o$ and He I $(1s4p)$ $^1P^o$ levels at lower impact velocities. Both Slim

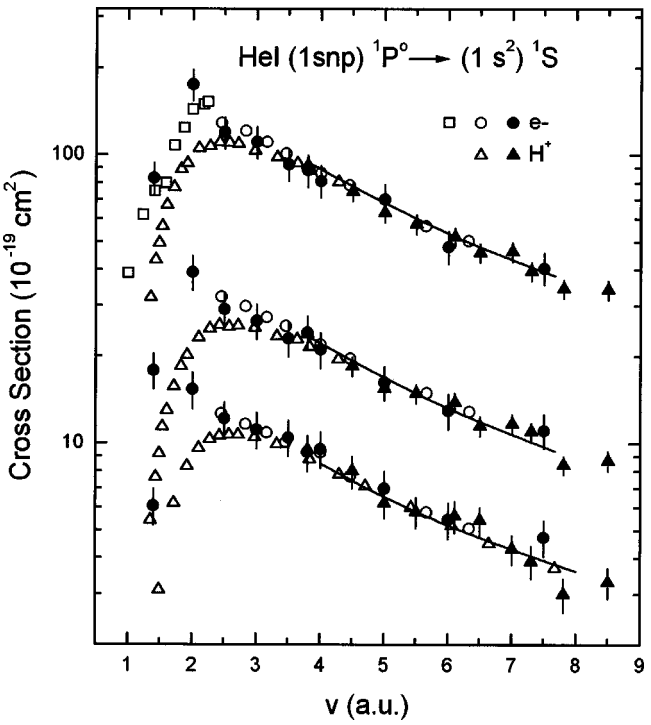

FIG. 3. A comparison of proton- and electron-impact data as a function of projectile velocity. $(1s2p)\ ^1P^o$ and $(1s3p)\ ^1P^o$: ● H^+ and ▲ e^- (corrected for polarization effects), this work; □ H^+, Park and Schowengerdt [41]; ○ H^+, Hippler and Schartner [27]; △ e^-, Westerveld *et al.* [28]. $(1s4p)\ ^1P^o$: Same as above except △ e^-, Donaldson *et al.* [26]; solid lines H^+, Bethe approximation [13] and Kim and Inokuti [42].

et al. and Fritsch appear to reproduce portions of oscillatory features in the lower-velocity experimental data; however, in the case of He I $(1s2p)\ ^1P^o$, they disagree strongly in terms of the phase and amplitude of the assumed oscillation. The differences between Slim *et al.*, Fritsch, and the present AOCC calculations lie essentially in the basis functions used. Fritsch used the one-electron approximation, which may not be adequate for the low-energy region, but has the possibility of adding many more basis functions in the calculations. In the calculations of Slim *et al.*, the basis sets on the projectile and the target are used and both electrons are included in the calculation. Our AOCC calculation is similar to that of Slim *et al.* except in the different choice of basis functions. We have included only basis functions on the target since we are more concerned with the higher-energy region. The lack of projectile basis functions in the expansion may account for the discrepancy of the present results with the other AOCC calculations at low energies. As explained earlier, the calculation of Fritsch was carried out with a one-electron model so that a larger basis set can be used in the close-coupling calculation. Slim *et al.* were more concerned with the electron-transfer channels and, since excitation is a weak process at low energies, the limited excitation channels used in their basis functions may give inadequate excitation cross sections. As seen from Fig. 2 the disparities between the experiments and among the theories in the low-energy region are still quite large. More elaborate calculations are needed to resolve these discrepancies.

Let us analyze the projectile dependence of the He I $(1snp)\ ^1P^o$ cross sections as a function of projectile velocity. In Fig. 3 we show a comparison of all the previously presented experimental data associated with electron and proton impact. As can be seen in this figure, the proton-induced cross sections are significantly larger with a maximum slightly shifted to lower velocities when compared to the corresponding electron data.

From Fig. 3 it can be seen that in the high-energy limit the e^- and H^+ projectile experimental results tend toward the first Born limit as expected. However, significant differences between electron and proton impact occur at velocities below 3 a.u. for the $(1snp)\ ^1P^o$ $(n=2-5)$ states, well outside the range of the error bars. In particular, it is observed that the cross sections for the excitation of helium by proton impact are larger than those obtained for electron impact. Additionally, the peak in the cross section for electron excitation is slightly displaced toward higher velocities compared to the proton results. In the lower-velocity region, electron-impact excitation results in a significant loss of the electron's incident energy. For proton impact such a loss is negligible. This may explain why electron-impact excitation cross sections are smaller than proton-impact excitation cross sections. It is important to note that these observed differences between electron and proton projectiles are probably not associated with a charge-state dependence of the excitation cross sections. Such a charge-state dependence could only be established on comparing electrons with positron impact or protons with antiproton impact.

B. Experimental cross-section results for molecular-hydrogen projectiles: H_2^+ and H_3^+

In this section we present our comprehensive EUV cross sections for the excitation of helium following H_n^+ ion impact for He I $(1snp)\ ^1P^o$, $n=1-3$, for projectile energies ranging from 50 to 400 keV/u, which correspond to velocities ranging from 1.4 to 4.0 a.u. A typical example of these experimental results for the He I $(1s3p)\ ^1P^o$ decays is shown in Fig. 4. For comparison, we have included optical measurements in the visible range from van den Bos *et al.* [15] and from Hasselkamp *et al.* [23,43], which cover a slightly larger velocity range. Good agreement with these results is observed for $v \geqslant 2.5$ a.u.. The cross sections for all He I $(1snp)\ ^1P^o \rightarrow (1s^2)\ ^1S$ transitions measured in this work are listed in Tables V for H_2^+ and VI for H_3^+ projectiles.

The observed difference at low velocities between the cross sections for H_3^+ and H_2^+ from this study and those from the other authors may be due to the pressure-dependent dissociation characteristics of these molecular species. Dissociation characteristics as a function of projectile energy and target pressure have been measured by Alvarez *et al.* [44] and by Williams and Dunbar [45]. These studies reveal that small fractions of neutral hydrogen and H^+ ions are produced in the dissociation of both H_3^+ and H_2^+ ions in addition to neutral H_2 and H_2^+ from the dissociation of H_3^+. The maximum production of such charge-screened species

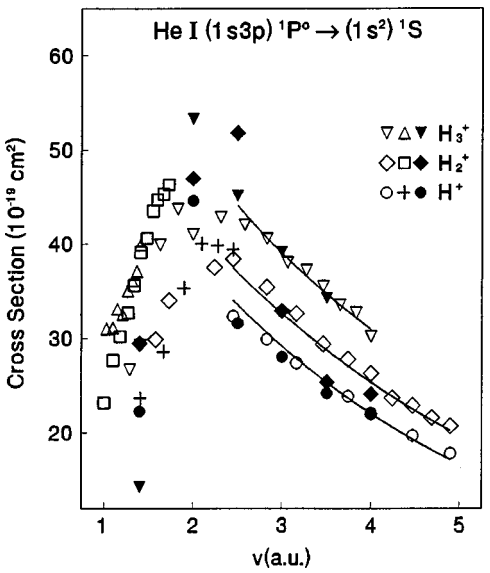

FIG. 4. A comparison of cross-section data for the excitation of the He I $(1s3p)\ ^1P^o$ state by H^+, H_2^+, and H_3^+ impact. ●, ◆, ▼=H^+, H_2^+, H_3^+, respectively, this work; +, □, △=H^+, H_2^+, H_3^+, van den Bos [15]; ○=H^+, Hippler and Schartner [27]; ◇, ▽=H_2^+, H_3^+, Hasselkamp *et al.* [23]. Curves are provided to guide the eyes.

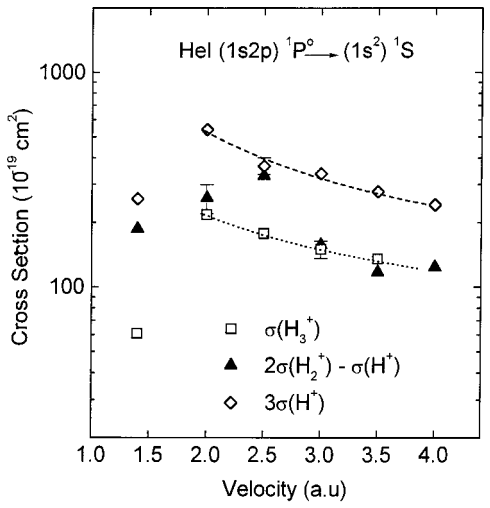

FIG. 5. Cross-section results for $\sigma^*(H_3^+)$ □, in comparison with results of the ''test equation,'' ▲ from the scaling model of Hasselkamp *et al.* [23], and scaled cross sections $3\sigma^*(H^+)$ ◇. Curves are provided to guide the eye.

occurs approximately at a target pressure of 10 mtorr and the lowest projectile energy presented in this study, the fraction moderately increasing below 50 keV and gradually decreasing for higher energies. While the charge fractions produced are small, predissociation of the projectile prior to encountering the emission region may explain the observed differences at low collision energies.

In addition, we have examined our EUV cross sections for H_n^+ ion impact with helium by comparing them first to the semiempirical scaling model of Hasselkamp [43]. At high H_n^+ impact velocities $v \geqslant 2$ a.u., we have observed that for the cross section for excitation (σ^*) by H^+, H_2^+, and H_3^+ ions the cross-section difference for $\sigma(H_3^+)$ and $\sigma(H_2^+)$ is approximately equal to the difference between $\sigma(H_2^+)$ and $\sigma(H^+)$, i.e.,

$$\sigma^*(H_3^+) - \sigma^*(H_2^+) \approx \sigma^*(H_2^+) - \sigma^*(H^+). \qquad (5)$$

This expression can be rearranged to read

$$\sigma^*(H_3^+) \approx 2\sigma^*(H_2^+) - \sigma^*(H^+). \qquad (6)$$

As an example we have plotted in Fig. 5 the cross sections for excitation of the $(1s2p)\ ^1P^o$ state of helium by H_3^+, the prediction of Eq. (5) referred to as the ''test'' equation [43], and proportionally scaled cross sections from H^+ impact. A sample of typical error bars has been included in this figure. For $v \geqslant 2$ a.u., we observe good agreement between the experimental data for $\sigma^*(H_3^+)$ and the ''test'' equation $2\sigma^*(H_2^+) - \sigma^*(H^+)$, while the proportionally scaled cross sections, namely, $3\sigma^*(H^+)$, are considerably larger than either of these quantities. In fact, interpreting excitation of He as a more distant collision phenomenon, screening by the projectile electrons is present, and an underproportionality is expected and in fact observed. At a projectile velocity of about $v = 1.3$ a.u. for H_3^+ the effective projectile electron energy is approximately equal to the excitation energies of the $(1snp)\ ^1P^o$ states and hence can be related directly to the energy defect for this projectile. However, for more distant collisions, the projectile electrons are not expected to contribute individually to the excitation process, and no contribution to the $\sigma^*(H_3^+)$ cross sections is apparent above this velocity, i.e., $\sigma^*(H_3^+)$ cross sections are consistently smaller than $3\sigma^*(H^+)$ results. To investigate electron-

TABLE V. Experimental EUV cross sections for the excitation of helium by H_2^+ impact, He I $(1snp)\ ^1P^o \rightarrow (1s^2)\ ^1S^o$, as a function of projectile velocity. Units are 10^{-19} cm^2.

Energy (keV)	Velocity (a.u.)	$(1s2p)\,^1P$	$(1s3p)\,^1P$	$(1s4p)\,^1P$	$(1s5p)\,^1P$
100	1.4	136±12	29.5±2.7	11.1±1.4	7.08±1.27
200	2.0	220±20	47.0±4.2	19.5±2.5	10.1±1.8
312	2.5	226±20	51.8±4.7	23.2±3.0	11.8±2.1
450	3.0	135±12	32.9±3.0	117.7±1.5	6.63±1.19
612	3.5	105±10	25.4±2.3	10.5±1.4	4.94±.90
800	4.0	102±9	24.1±2.2	10.5±1.4	6.25±1.13

TABLE VI. Experimental EUV cross sections for the excitation of helium by H_3^+ impact, He I $(1snp)\ ^1P^o \rightarrow (1s^2)\ ^1S^o$, as a function of projectile velocity. Units are 10^{-19} cm^2.

Energy (keV)	Velocity (a.u.)	$(1s2p)\,^1P$	$(1s3p)\,^1P$	$(1s4p)\,^1P$	$(1s5p)\,^1P$
150	1.4	60.8±5.5	14.3±1.3	5.46±.71	3.02±.54
300	2.0	217±20	53.3±4.8	19.4±2.5	11.3±2.0
468	2.5	178±16	45.1±4.1	17.1±2.2	10.6±1.9
674	3.0	150±14	39.1±3.5	13.3±1.7	7.48±1.35
918	3.5	135±12	34.3±3.1	14.9±1.9	8.17±1.47

screening effects we have also analyzed the ratios $\sigma^*(H_3^+)/3\sigma^*(H^+)$ and $\sigma^*(H_2^+)/2\sigma^*(H^+)$ for the transitions He I $(1snp)\ ^1P^o \rightarrow (1s^2)\ ^1S$, $n=2-5$.

In general our results indicate that the scaling model of Hasselkamp *et al.* is applicable for the corresponding projectile velocities in this study. However, by examining the ratios of $\sigma^*(H_n^+)$ to $n\sigma^*(H^+)$, the limitations associated with treating H_n^+ as a mixture of independent particle beams is clearly revealed. Since a more refined theoretical description of such complex multicenter collision processes does not currently exist, little can be said about contributions to the total scattering amplitude due to multicenter scattering and interference effects.

V. CONCLUSION

Comprehensive cross-section measurements involving excitation of He I $(1snp)\ ^1P^o$ $(n=2-5)$ states have been performed using electron, proton, H_2^+, and H_3^+ projectiles over a large velocity range under the same experimental conditions. In the high-energy limit our cross sections for electron and proton impact merge together as expected. However, the maximum of the cross sections for electron excitation of helium is shifted to a slightly higher energy with respect to the maximum for the proton case. This may be due to a mass effect, which leads to different threshold velocities for electrons and protons.

Furthermore, advanced convergent close-coupling, *R*-matrix, and atomic-orbital close-coupling methods have been used to calculate excitation cross sections at a wide range of projectile velocities. These results nicely reproduce our EUV data at the intermediate energies and are in excellent agreement with previous electron measurements corresponding to the low-energy range. In contrast, although AOCC results agree well with the experimental data at intermediate proton-impact energies, disparities between experimental cross sections and these theoretical predictions in the low-energy region are still quite large, demanding more elaborate calculations in order to resolve these differences.

For molecular projectiles, we have found good agreement between the experimental data and the ''test'' equation of the scaling model. However, our measured cross-section ratios clearly reveal the contribution of dynamical effects, including screening, by the molecular electrons, since a proportional scaling of 1:1 for $n\sigma^*(H^+)$ and $\sigma^*(H_n^+)$, $n=2$ and 3, is never attained. Finally, the present study may provide a comprehensive database for the test of theoretical atomic and molecular collision models.

ACKNOWLEDGMENTS

We would like to thank Dr. Silvano Fineschi from the Harvard-Smithsonian Center for Astrophysics for many interesting discussions and fruitful suggestions. We would like also to express our gratitude to Dr. W. Fritsch from the Hahn-Meitner-Institut, Berlin, for his valuable suggestion to use the AOCC method for proton impact. This work was supported, in part, by the National Science Foundation (K.B.), the Nevada Business and Science Foundation, and ACSPECT Corporation, Reno, Nevada.

[1] J. H. McGuire, Adv. At., Mol., Opt. Phys. **29**, 217 (1992).
[2] R. Bruch, E. Rauscher, S. Fülling, D. Schneider, S. Mannevik, and M. Larsson, *Molecular And Atomic Collision Processes With Ion Beams*, Vol. 10 of *Encyclopedia of Applied Physics* (VCH, Weinheim, 1994), p. 437.
[3] J. H. McGuire, *Electron Correlation Dynamics In Atomic Collisions* (Cambridge University Press, Cambridge, 1997).
[4] R. C. Mancini, C. F. Hooper, Jr., N. D. Delamater, A. Hauer, C. J. Keane, B. A. Hammel, and J. K. Nash, Rev. Sci. Instrum. **63**, 5119 (1992).
[5] S. Fineschi, R. B. Hoover, J. M. Fontela, and A. B. C. Walker, Opt. Eng. (Bellingham) **30** (8), 1161 (1991).
[6] H. P. Summer, M. von Hellermann, P. Breger, J. Frieling, L. D. Horton, R. Konig, W. Mandel, H. Morsi, R. Wolf, F. de Heer, R. Hoekstra, and W. Fritsch, Joint European Torus Publication (JET) No. 48, 1991 (unpublished).
[7] F. J. de Heer, R. Hoekstra, and H. P. Summers, Joint European Torus Publication (JET) No. 47, 1992 (unpublished).
[8] F. J. de Heer, R. Hoekstra, A. E. Kingston, and H. P. Summers, Joint European Torus Publication (JET) No. 19, 1992 (unpublished).
[9] F. J. de Heer, R. Hoekstra, and H. P. Summers, Nucl. Fusion Suppl. **3**, Suppl. S, 47 (1992).
[10] W. Fritsch, Nucl. Fusion Suppl. **3**, Suppl. S, 41 (1992).
[11] F. J. de Heer, International Nuclear Data Committee Report No. IDC(NDS)-385 Vienna, Austria, 1998 (unpublished).
[12] S. A. Kazantsev, N. M. Firstova, A. G. Petrashen, J.-C. Henoux, and A. V. Bolatov, Opt. Spektrosk. **78**, 729 (1995) [Opt. Spectrosc. **5**, 655 (1995)].
[13] K. L. Bell, D. J. Kennedy, and A. E. Kingston, J. Phys. B **1**, 1037 (1968).
[14] M. Inokuti, Rev. Mod. Phys. **43**, 297 (1971).
[15] J. van den Bos, Phys. Rev. **181**, 191 (1969); J. van den Bos, G. J. Winter, and F. J. de Heer, Physica (Amsterdam) **40**, 357 (1968); **44**, 143 (1969).
[16] H. A. Slim, E. L. Heck, B. H. Bransden, and D. R. Flower, J. Phys. B **24**, 1683 (1991).
[17] W. Fritsch, Phys. Lett. A **160**, 64 (1991).
[18] D. V. Fursa and I. Bray, Phys. Rev. A **52**, 1279 (1995).
[19] D. V. Fursa and I. Bray, J. Phys. B **30**, 757 (1997).
[20] K. Bartschat, E. T. Hudson, M. P. Scott, P. G. Burke, and V. M. Burke, J. Phys. B **29**, 2875 (1996).
[21] E. T. Hudson, K. Bartschat, M. P. Scott, P. G. Burke, and V. M. Burke, J. Phys. B **29**, 5513 (1996).
[22] W. Fritsch and C. D. Lin, Phys. Rep. **201**, 1 (1991).
[23] D. Hasselkamp, S. Hippler, A. Scharmann, and K.-H. Schartner, Z. Phys. D: At., Mol. Clusters **6**, 269 (1987).
[24] M. Bailey, R. Bruch, E. Rauscher, and S. Bliman, J. Phys. B **28**, 2655 (1995).
[25] M. Bailey, MS thesis, University of Nevada, Reno, 1992.

[26] F. G. Donaldson, M. A. Hender, and J. W. McConkey, J. Phys. B **5**, 1192 (1972).
[27] R. Hippler and K.-H. Schartner, J. Phys. B **7**, 618 (1974).
[28] W. B. Westerveld, H. G. M. Heideman, and J. van Eck, J. Phys. B **12**, 115 (1979).
[29] W. Stolte, Ph.D. thesis, University of Nevada, Reno, 1994.
[30] W. Stolte and R. Bruch, Phys. Rev. A **54**, 2116 (1996).
[31] H. Merabet, M. Bailey, R. Bruch, D. V. Fursa, I. Bray, J. W. McConkey, and P. Hammond, Phys. Rev. A **60**, 1187 (1999).
[32] H. Merabet, A. Siems, R. Bruch, S. Fülling, M. Bailey, Proc. SPIE **3764**, 2 (1999).
[33] A. Götz, W. Mehlhorn, A. Raeker, and K. Bartschat, J. Phys. B **29**, 4699 (1996).
[34] H. Merabet, A. Siems, J. Hanni, R. Bruch, S. Fülling, M. Bailey, Proc. SPIE **4139**, 80 (2000).
[35] W. C. Fon, K. A. Berrington, P. G. Burke, and A. E. Kingston, J. Phys. B **14**, 1041 (1981).
[36] K. A. Berrington and A. E. Kingston, J. Phys. B **20**, 6631 (1987).
[37] P. M. J. Sawey and K. A. Berrington, At. Data Nucl. Data Tables **55**, 81 (1993).
[38] K. Bartschat, E. T. Hudson, M. P. Scott, P. G. Burke, and V. M. Burke, Phys. Rev. A **54**, R998 (1996).
[39] K. Bartschat, Comput. Phys. Commun. **114**, 168 (1998).
[40] K. Bartschat, J. Phys. B **31**, L469 (1998).
[41] J. T. Park and F. D. Schowengerdt, Phys. Rev. **185**, 152 (1969).
[42] Y.-K. Kim and M. Inokuti, Phys. Rev. **175**, 176 (1968); **184**, 38 (1969).
[43] D. Hasselkamp, Ph.D. thesis, University of Giessen, Germany, 1976.
[44] I. Alvarez, C. Cisneros, C. F. Barrett, and J. A. Ray, Phys. Rev. A **14**, 602 (1976).
[45] J. F. Williams and D. N. F. Dunbar, Phys. Rev. **149**, 62 (1966).